IEEE Access
Multidisciplinary | Rapid Review | Open Access Journal

Received 2 October 2023, accepted 31 October 2023, date of publication 6 November 2023, date of current version 9 November 2023.

Digital Object Identifier 10.1109/ACCESS.2023.3330236

RESEARCH ARTICLE

All-Optical UAV-Based Triple-Hop FSO-FSO-VLC Cooperative System for High-Speed Broadband Internet Access in High-Speed Trains

AARTHI GUNASEKAR[1], L. BHARGAVA KUMAR[2], PRABU KRISHNAN[3], (Senior Member, IEEE), RAJESH NATARAJAN[1], AND DUSHANTHA NALIN K. JAYAKODY[4], (Senior Member, IEEE)

[1]Department of Communication Engineering, Vellore Institute of Technology, Vellore 632014, India
[2]Department of Electronics and Communication Engineering, BVRIT Hyderabad College of Engineering for Women, Hyderabad, Telangana 500090, India
[3]Department of Electronics and Communication Engineering, National Institute of Technology Karnataka, Surathkal 575025, India
[4]COPELABS, Lusófona University, 1700-097 Lisbon, Portugal

Corresponding author: Aarthi Gunasekar (aarthi.g@vit.ac.in)

ABSTRACT In this paper, we proposed an unmanned aerial vehicle (UAV) based all optical triple hop mixed free space optical-free space optical-visible light communication (FSO-FSO-VLC) system for broadband internet access in high-speed train applications. The system consists of triple hops from gateway to the UAV, UAV to train and train to the end user. Two decode and forward relays are mounted on the UAV and train respectively to transmit the data between the gateway to the end-users. The first hop between gateway to UAV consist of FSO link which follows M-distribution. The second hop between the UAV to train consists of FSO link and is modelled using Gamma-Gamma distribution which takes into account both atmospheric turbulence and pointing errors due to position/orientation deviation. The third hop between the train and end user is connected using VLC link and it is mathematically modelled using Lambertian emission distribution. The relays map the incoming signal on the FSO links and send it down to the user inside the train via the VLC downlink. We derived the closed form expressions for average bit error rate and outage probability of the proposed system. This paper investigates the effects of atmospheric turbulence, field of view, beam divergence angle, displacement deviation variance, optical concentrator gain, number of access point, and modulation schemes on system performance. First time, we proposed all-optical system which offers high data rate and low transmission delay.

INDEX TERMS FSO, UAV, VLC, atmospheric turbulence, outage probability, average BER, M-distribution, gamma-gamma.

I. INTRODUCTION

The development of broadband internet services in high-speed train (HST) systems has been necessitated by the deployment of HST systems and improved technology, as well as the need for continuous internet access in any environment. The increasing popularity of internet-connected digital devices places a premium on reliable and fast internet connectivity in HSTs. There is an ongoing demand for higher bit rates to propel the development of optical wireless communication (OWC) technologies in order to meet the demands of wireless communication applications. The forthcoming decade is projected to witness a significant increase in HSTs with significant advancements over existing technology. Since trains are the largest passenger and goods-carrying vehicles for long distances economically, they need upgrades with the developing technology. Many of the countries are providing internet services for travelers in their high-speed or metro trains. These trains have several benefits: reduction in travel time, vehicle operating cost, pollution,

The associate editor coordinating the review of this manuscript and approving it for publication was Halil Ersin Soken.

© 2023 The Authors. This work is licensed under a Creative Commons Attribution-NonCommercial-NoDerivatives 4.0 License.
For more information, see https://creativecommons.org/licenses/by-nc-nd/4.0/

accidents, etc. Also, these trains have enhanced safety, job creation, tourism development, and growth in the country's gross domestic product (GDP) [1], [2].

Trains with modern and enhanced facilities are always recommended and supported by the passengers. Trains experience frequent switching in their communications to the ground as they move at higher speeds. Such trains with OWC systems give exceptional performance and make them intelligent transport systems (ITS). OWC systems have several benefits, such as high bandwidth, high security, license-free spectrum, and economical when compared to radio frequency (RF) communication systems [3], [4]. Recently, there has been a significant improvement in the relay-assisted communication systems due to increased communication distance, strengthening network connectivity with enhanced reliability. People use either a moving/flying relay or a ground-based relay in this modern world, depending on the application [5].

Operating an HST with free space optics (FSO) link - based ground-to-train communication gives several difficulties for the railway operators. A few of these difficulties are the requirement of substantial working capital, more base stations (BSs), uninterrupted connectivity. All three things are related to each other to make the communication system effective and efficient. The uninterrupted ground-to-train connectivity comes with more base stations with which the operational cost increases. To make the communication system economical, one should reduce the number of BSs by extending the link length with enhanced coverage. Handover delay is another important factor that makes the communication system inefficient and interrupts the data services [6]. An efficient communication system should have a minimal handover delay. When the train moves at high speed, it encounters frequent handovers by switching the connections between the BSs [7], [8]. The impact of track irregularities and train movement creates misalignment fading and requires an acquisition-tracking-pointing (ATP) system to mitigate the effect of fading. A wide-angle FSO beam can be employed at the BSs to enhance the communication system performance [9].

There are enormous hybrid and relay-assisted works in the past related to the OWC systems. Still, the researchers are extending their works in many fields with new approaches. In [19] authors proposed and analyzed the performance of a relay-assisted FSO system to give ground to train communications and relays the data to the following base stations. The system uses all-optical amplify and forward (AOAF) and AOAF with optical and optical-electronical-optical (OEO) recovery schemes. In [20], the authors proposed a dual transceivers scheme, which uses two transceivers on both base stations and trains to lower system costs and achieve seamless handovers. A wide beam was used to implement FSO communications in order to improve the reliability and reduce the design complexity of a ground-to-train FSO system.

Khallaf et al. studied and proposed the unmanned aerial vehicles (UAVs)-based FSO communication system for HSTs backhauling [21], [22]. The authors in [23] proposed the bit error rate (BER) analysis of polarization shift keying (POLSK) based FSO link for inter UAV communication over different weather conditions. In [24], the authors made outage probability analysis of FSO-based inter UAV communication over lognormal and gamma-gamma (GG) channel models. They also performed the average BER (ABER) analysis for the binary phase-shift keying (BPSK) modulation scheme. I Swamidoss et al. proposed FSO communication for UAV applications for high-speed communications and investigated the average spectral efficiency (ASE) using various modulation schemes such as POLSK, On-Off Keying (OOK), and Coherent Optical Wireless Communication [25]. In [26], the authors also analyzed the BER performance of FSO communication links with various data rates, and wavelengths from UAV to the ground station to improve data communication performance under different weather conditions of United Arab Emirates. The outage and bit error rate performance of the system was analyzed using the closed-form expressions. The channel modeling, performance analysis and parameter optimization of the hovering UAV-based FSO communication is studied in [27], [28], and [29]. To meet the increasing demand for uninterrupted internet connectivity with high data rates 24/7 everywhere, a solution named Free-space OptiCs Utilization (FOCUS) for HSTs presented in [30].

Xu et al. proposed a unified UAV-based dual-hop FSO/FSO system with the AF relaying protocol and IMDD technique using Gamma-Gamma and Málaga distribution channels [31], [32]. The authors in [33] proposed a mixed FSO/RF system, which enables communication from a ground central unit (CU) to multiple ground users (GUs) over a hovering UAV and acts as a DF relay. The relay communicates with the GUs over multiple-input multiple-output (MIMO) RF links with orthogonal space-time block coding (OSTBC) transmission. To analyze the outage probability, the authors employed Nakagami/Inverse Gamma (IG) composite fading channels for the RF links and MIMO channels. Lu et al. proposed a hovering UAV-based dual-hop FSO system using a DF relay with multiple sources. The authors also suggested an optimization algorithm to improve the system performance significantly [34]. The authors in [35] analyzed the performance of a UAV-assisted multi-hop hybrid FSO/RF communication system where the FSO and RF links suffer with the Exponential Weibull turbulence model and the Nakagami fading model.

In [36], Paudel et al. experimentally demonstrated a ground-to-train system using FSO communication link in the lab environment to provide high-speed broadband services on HSTs. The authors analyzed the performance of the prototype system in terms of Q-factor along the rail track. To reduce the impact of handovers in ground-to-train FSO Communications, RotAting TranscEiver (RATE) scheme

TABLE 1. Comparison of proposed work with other technologies.

References	Technology	Data Rate	Analyzed Parameters	Number of hops	Ground-to-Train Link	Inside Train Link	Drawbacks
[2]	IEEE802.16e IEEE802.16m	65 kbps	End-to-end Delay, Throughput	1	WiMax	-	Very very low data rate, Frequent handoffs
[10]	Satellite	Uplink–512 kbps Downlink–2 Mbps	-	3	RF	Wi-Fi	Very low data rate, poor coverage area in hilly regions, No coverage inside the tunnels
[11]	IEEE 802.20, Wireless wide area network (WWAN)	2 Mbps	-	2	WWAN	-	Low data rate, Frequent handoffs
[12]	Radio over fiber (ROF)	0.5 Gbps to 5 Gbps	Switching and handover time	2	Fiber/RF	-	High frequent handoffs, Low flexibility
[13]	Leaky coaxial cable (LCX)	768 kbps	-	3	Ethernet & LCX	Wi-Fi	Very low data rate, Frequent handoffs
[14]	FSO	566 Mbps	Handover time	2	FSO	-	-
[15]	UAV-aided SWIPT	-	Ergodic outage probability	2	RF	-	Low data rate, Frequent handoffs
[16]	IRS-assisted UAV	45 Mbps	Minimum data rate	2	RF	-	Low data rate, Frequent handoffs
[17]	UAV	-	-	2	RF	-	Low data rate, Frequent handoffs
[18]	Multi UAV based on machine learning	50 Mbps	Data rate	2	RF	-	Low data rate, Frequent handoffs
Proposed work	UAV-based cooperative FSO-FSO-VLC (First time we proposed)	1 Gbps	ABER, Outage probability	3	FSO	VLC	-

TABLE 2. List of variables.

Variable	Description
C_n^2	Refractive index structure parameter
ξ	Pointing error parameter of the First-hop link
k	Magnitude of spatial frequency
L	FSO Link range
L_V	Height of LED
$n(t)$	AWGN noise
p	Detection type
P_t	Transmitted power
q	Modulation parameter
R	APD responsivity for FSO link
R_p	APD responsivity for VLC link
Z	UAV Height
L_c	Coverage distance of the train track
P_e	Average bit error rate
P_{e2e}	End-to-end Average bit error rate
α_1, β_1	FSO turbulence parameters of first-hop
α_2, β_2	FSO turbulence parameters of second-hop
$\Gamma(.)$	Gamma function
λ	Wavelength
σ_R^2	Rytov variance
γ_{th}	Threshold SNR
h_t	Fading due to turbulence
h_p	Pointing loss
h_l	Path loss

and optimal positioning of ground base stations methods proposed in [37] and [38].The authors in [39] proposed and studied the enhancement of the link range of FSO-based ground-to-train communication using multiple transmitters for a high data rate. In order to increase the system performance the FSO system should be augmented with visible light communication (VLC) system which offers improved data rates for indoor communications. In [40], cascaded FSO-VLC communication was proposed consisting of multiple VLC access points catering the end users connected to FSO backhaul link. In [41], solutions for last mile access network bottleneck issues were experimentally illustrated using hybrid FSO-VLC link. The outage probability of RF-FSO-VLC system is analyzed in [42], which shows good system performance at high optical power.

Uninterrupted Internet connectivity is a growing demand for onboard passengers worldwide, necessitating the inclusion of high-speed broadband internet services in HSTs. This prompted the development of a triple-hop all-optical cooperative FSO-FSO-VLC system to meet the growing demand for high-speed broadband internet access in high-speed trains. According to the literature, internet access technologies for HST applications include RF, satellite communication, coaxial cable, radio over fibre (RoF) for ground-to-train communication, and Wi-Fi inside the train. Thus, the significant disadvantages of these existing technologies are the increased number of handoffs, the low

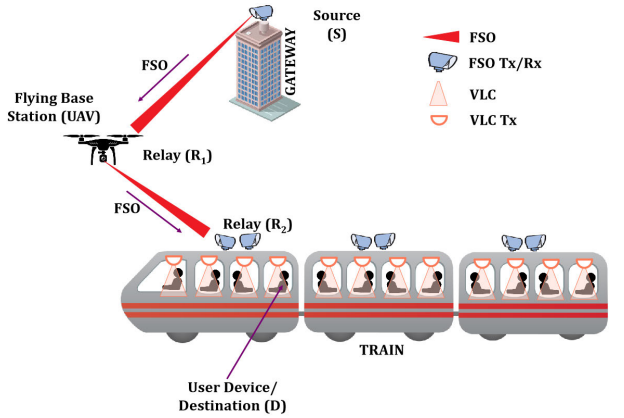

FIGURE 1. Generalized triple-hop FSO-FSO-VLC system.

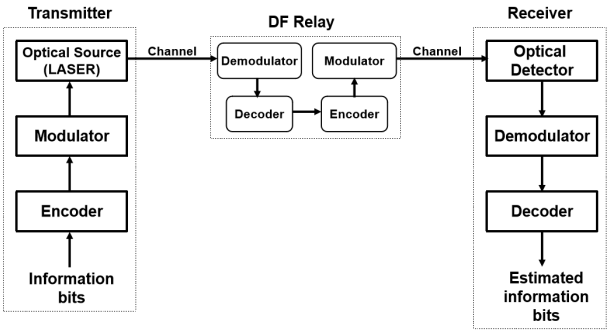

FIGURE 2. Wireless optical communication system with a DF relay.

data rate, and the high delay. Through a triple-hop UAV-based FSO-FSO-VLC all-optical link, we overcome the disadvantages of existing technologies in the literature by providing a high data rate and low transmission delay. The VLC link is added as an access network for the train's passengers' devices. We analyzed the outage and ABER performance of the end-to-end system using the closed-form expressions. The proposed triple-hop system is compared to other technologies mentioned in the literature in Table 1.

Section II explains the UAV-assisted triple-hop FSO-FSO-VLC cooperative communication system model. Section III gives the FSO and VLC statistical channel models for the proposed triple-hop system. Section IV gives the performance analysis in terms of average bit error rate (ABER) and outage probability. Section V shows the results and discussions. This paper concludes in Section VI. Table 2 shows all the variables used in the calculations.

II. SYSTEM MODEL

The new technology metro trains require high-speed internet connectivity for the people utilizing them. Modern equipment with advanced technologies brings it into a real-time environment. We considered a triple-hop system as shown in Fig. 1 with two relay nodes.

The first relay node, R_1 is mounted on the UAV. The second relay node R_2 is on the top of the train. The source gateway

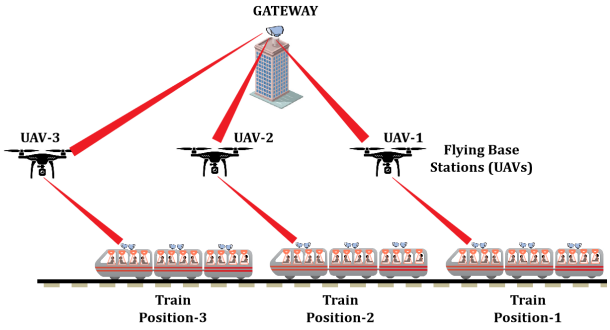

FIGURE 3. Positioning of UAV relay base stations according to the HST positions.

(S) to the user device/destination (D) inside the train makes a complete triple-hop system with two decode and forward (DF) relay nodes. The first two hops use FSO communication, and the third hop uses VLC.

Fig. 2 depicts the block diagram of a relay-assisted communication system with a DF relay. The bits of information are encoded with the encoder, modulated, and then transmitted with a laser diode. The DF relay contains modulator/demodulator and encoder/decoder units to perform operations such as receiving and re-transmitting decoded and encoded bits of information. The optical photo detector captures the received light signal and converts the intensity fluctuations into electrical signals at the receiver. They are then demodulated and decoded in order to estimate the bits of information [43].

The positioning of UAV relay base stations based on the HST positions is depicted in Fig. 3. The UAV serves as a flying base station or flexible relay node, responsible for receiving the signal transmitted from the gateway and transmitting it to the HST. In the proposed system, three UAV's are strategically positioned at various locations along the train in order to facilitate the transmission and reception of signals to the HST. The UAV's 1, 2 and 3 covers the train positions 1, 2 and 3 respectively. Depending on the required distance, the number of UAV's can be expanded and located at various positions along the rail track to provide internet connectivity.

The electrical signal received at the DF based relay R_1 is given by

$$y_{R_1} = h_1 P_t R x + n, \tag{1}$$

where $h_1 = h_t\, h_p\, h_l$ is the irradiance, in which h_t represents the fading due to atmospheric turbulence, h_p represents the pointing loss, and h_l is the path loss. P_t denotes the transmitted power, R is the responsivity, x is the signal transmitted from the source (S), and n is the additive white gaussian noise (AWGN) with zero mean and variance $\sigma^2_{R_1}$. Similarly, the received signal at DF relay R_2 is given as

$$y_{R_2} = R h_2 P_t \hat{x}_1 + n, \tag{2}$$

where h_2 denotes the irradiance of the link between relay nodes R_1 and R_2, $\hat{x}_1$ is the signal transmitted from the relay R_1. The electrical signal received at the user device/destination (D) is given as

$$y_D = Rh_3P_t\hat{x}_2 + n. \tag{3}$$

where h_3 denotes the direct current (DC) channel gain of the line of sight (LOS) link between the relay R_2 and the destination (i.e, VLC user device), $\hat{x}_2$ is the signal decoded at VLC user device.

III. STATISTICAL CHARACTERISTICS

A. GATEWAY TO UAV

A Malaga distributed FSO link employed in between the source gateway and UAV (relay-1). The physical channel model of the M-distribution includes three components, namely, the LOS component U_L, and scattered components U_S^C and U_S^G (see Fig.1 of [44]). The component U_S^C is coupled to the LOS contribution and scattered by the eddies on the propagation axis. The component U_S^G is independent of the LOS contributions and spread by the off-axis eddies. The parameters $\Omega = E[|U_L|^2]$, $\rho 2b_0 = E[|U_S^C|^2]$, and $g = E[|U_S^G|^2] = 2b_0(1-\rho)$ denote the average power of these three components. The parameter ρ denotes the amount of scattering power coupled to the LOS component and ranges from 0 to 1. The total average power of the scattered components is $2b_0 = E[|U_S^C|^2 + |U_S^G|^2]$. Here $E[\cdot]$ represents the mean or expected average value of the parameter. The parameter Ω' in Eq.(4) is the average power from the coherent contributions and mathematically given as $\Omega' = \Omega + 2\left(\rho b_0 + Cos(\Phi_A - \Phi_B)\sqrt{2\rho b_0}\right)$. The angles Φ_A and Φ_B are related to the components U_L and U_S^C respectively. The probability density function (PDF) of the receiver irradiance h_1 for the M-distributed channel with turbulence, path loss h_l and pointing error is given as ([45], Eq.(5))

$$f_{h_1}(h) = \frac{\xi^2 A}{2\,h_1}\sum_{m=1}^{\beta_1} b_m\, \mathrm{G}_{1,3}^{3,0}\left[\frac{\alpha_1\,\beta_1}{(g\,\beta_1+\Omega')}\frac{h_1}{h_l\,A_0}\middle|\begin{matrix}\xi^2+1\\ \xi^2,\alpha_1,m\end{matrix}\right], \tag{4}$$

where $\mathrm{G}_{p,q}^{m,n}[\cdot]$ denotes the Meijer-G function. Using the random variable transformation, for the Intensity modulation/Direct detection (IM/DD) scheme, the Eq. (4) is given in terms of Signal-to-Noise ratio (SNR) as ([45], Eq.(7))

$$f_{\gamma_1}(\gamma) = \frac{\xi^2 A}{4\,\gamma}\sum_{m=1}^{\beta_1} b_m\, \mathrm{G}_{1,3}^{3,0}\left[B\sqrt{\frac{\gamma}{\mu}}\middle|\begin{matrix}\xi^2+1\\ \xi^2,\alpha_1,m\end{matrix}\right], \tag{5}$$

where $b_m = a_m\left[\frac{\alpha_1\beta_1}{g\beta_1+\Omega'}\right]^{-\frac{\alpha_1+m}{2}}$, $B = \frac{\xi^2\alpha_1\beta_1\,(g+\Omega')}{[(\xi^2+1)(g\beta_1+\Omega')]}$, and the electrical SNR is

$$\mu = \frac{\xi^2\left(\xi^2+1\right)^{-2}\left(\xi^2+2\right)\left(g+\Omega'\right)}{(1+1/\alpha_1)\left[2\,g\,(g+2\,\Omega')+\Omega'^2\,(1+1/\beta_1)\right]}\,\bar{\gamma}_1, \tag{6}$$

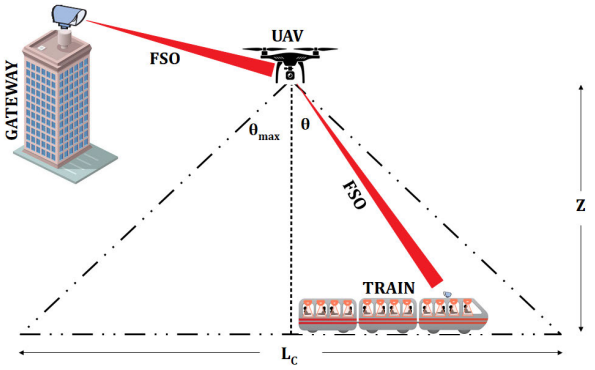

FIGURE 4. Geometrical representation of UAV to train.

Here the parameter $\bar{\gamma}_1$ represents the average SNR of the Malaga distributed FSO channel.

$$A \triangleq \frac{2\,\alpha_1^{\alpha_1/2}}{g^{1+\alpha_1/2}\Gamma(\alpha_1)}\left(\frac{g\,\beta_1}{g\,\beta_1+\Omega'}\right)^{\beta_1+\alpha-1/2},$$

$$a_m \triangleq \binom{\beta_1-1}{m-1}\frac{\left(g\,\beta_1+\Omega'\right)^{1-m/2}}{(m-1)!}\left(\frac{\Omega'}{g}\right)^{m-1}\left(\frac{\alpha_1}{\beta_1}\right)^{m/2},$$

The cumulative distribution function (CDF) of the Eq. (5) is ([45], Eq.(12))

$$F_{\gamma_1}(\gamma) = \frac{\xi^2 A}{8\pi}\sum_{m=1}^{\beta_1} b_m\, 2^{\alpha_1+m-1}\,\mathrm{G}_{3,7}^{6,1}\left[\frac{B^2}{16}\,\frac{\gamma}{\mu}\middle|\begin{matrix}X\\ Y\end{matrix}\right], \tag{7}$$

where

$$X = 1, \frac{\xi^2+1}{2}, \frac{\xi^2+2}{2}, \text{ and}$$
$$Y = \frac{\xi^2}{2}, \frac{\xi^2+1}{2}, \frac{\alpha_1}{2}, \frac{\alpha_1+1}{2}, \frac{m}{2}, \frac{m+1}{2}, 0.$$

B. UAV TO TRAIN

From the UAV to the train, the communication link uses Gamma-Gamma (GG) turbulence with misalignment fading. Fig. 4 shows the geometrical representation of the UAV to train channel. The height of the UAV from ground is Z metre, which connects the HST at a coverage distance of $L_c = 2Ztan(\theta_{max})$ metre of the train track.The FSO link length $d = \frac{Z}{cos(\theta)}$, where θ, is the angle between the UAV altitude Z and the FSO link. The UAV aperture orientation changes randomly, whereas the HST aperture orientation is assumed to be fixed taking into consideration a more steady platform.

The PDF of the gamma-gamma distribution with turbulent induced fading h_t and path loss h_l is given by ([46], Eq.(10))

$$f_{h_t}(h) = \frac{(\alpha_2\beta_2)^{\frac{(\alpha_2+\beta_2)}{2}}\,h_t^{\frac{(\alpha_2+\beta_2)}{2}-1}}{\Gamma(\alpha_2)\Gamma(\beta_2)h_l^{\frac{(\alpha_2+\beta_2)}{2}}}G_{0,2}^{2,0}\left[\alpha_2\beta_2\frac{h_t}{h_l}\middle|\begin{matrix}-\\ \frac{(\alpha_2-\beta_2)}{2},\frac{(\beta_2-\alpha_2)}{2}\end{matrix}\right] \tag{8}$$

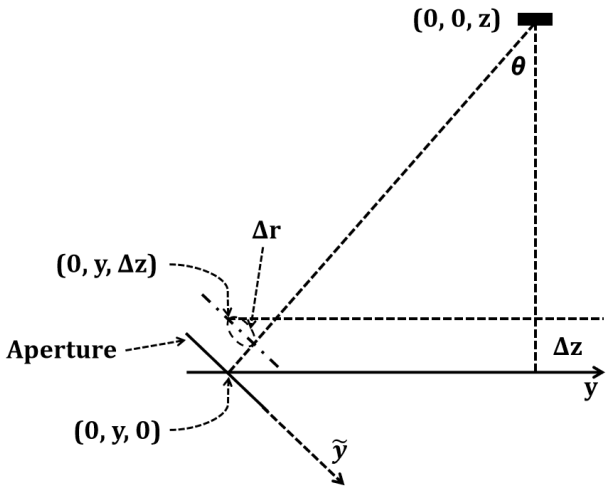

FIGURE 5. Illustration of vertical shift in the train location by Δz.

where $\Gamma(\cdot)$ represents the gamma function.The turbulence parameters are α_2 ([47], Eq.(18)) and β_2 ([47], Eq.(19)) given as

$$\alpha_2 = \left[\exp\left(\frac{0.49\sigma_R^2}{\left(1 + 1.11\sigma_R^{12/5}\right)^{7/6}} \right) - 1 \right]^{-1}, \tag{9}$$

$$\beta_2 = \left[\exp\left(\frac{0.51\sigma_R^2}{\left(1 + 0.69\sigma_R^{12/5}\right)^{5/6}} \right) - 1 \right]^{-1}, \tag{10}$$

where σ_R^2 is the Rytov variance for a vertical FSO link between the HST and the UAV given as ([21], Eq.(3)).

$$\sigma_R^2 = 2.24k^{\frac{7}{6}}(\sec(\theta))^{\frac{11}{6}} \int_0^Z C_n^2(z) z^{\frac{5}{6}} dz, \tag{11}$$

where z is the height in meters, $k = \frac{2\pi}{\lambda}$ is the wave number, and λ is the wavelength. $C_n^2(z)$ is the refractive index structure constant given by ([21], Eq.(4))

$$C_n^2(z) = 0.00594 \left(\frac{W}{27}\right)^2 \left(10^{-5} z\right)^{10} \exp(-z/1000) + 2.7 \times 10^{-16} \exp(-z/1500) + A \exp(-z/100) \tag{12}$$

where W^2 indicates the mean square value of the wind speed in m/s, A represents the value of $C_n^2(0)$ at ground.

Despite the fact that both trains and UAVs have ATP systems, in practise the variations brought on by train motion and UAV hovering cannot be adequately adjusted.These variations cause the position of the received beam at the receiver aperture to vary. Fig. 5 uses the example of a vertical movement in the train location by distance Δz to demonstrate the impact of vibration on the location of the received beam.

The best position for the train and the UAV are $(0, 0, Z)$ and $(0, y, 0)$, respectively, if ATP system operates flawlessly and offers full compensation. However, in reality, for both UAV and train, these positions switch to $(\Delta x_D, \Delta y_D, Z + \Delta z_D)$ and $(\Delta x_T, y + \Delta y_T, \Delta z_T)$, respectively. Δx_D, Δy_D, Δz_D, Δx_T, Δy_T, and Δz_T are independent zero-mean Gaussian random variables with variance of σ_p^2. Additionally, the orientation of the UAV aperture randomly shifts from $\{\theta, 0\}$ in z-y plan and z-x plan to $\{\theta + \Delta\theta, \Delta\phi\}$ where $\Delta\theta$ and $\Delta\phi$ are zero-mean independent Gaussian random variables with variance σ_θ^2.

The radial displacements caused by these vibrations in position and orientation are provided, respectively, in the directions of the x and $\tilde{y}$ axis by ([21], Eq.(5) and Eq.(6)) $\Delta r_x = \Delta x_T + \Delta x_D + \frac{\Delta\phi Z}{\cos(\theta)}$, $\Delta r_{\tilde{y}} = (\Delta z_T + \Delta z_D)\sin(\theta) + (\Delta y_T + \Delta y_D)\cos(\theta) + \frac{\Delta\theta Z}{\cos(\theta)}$. The pdf of the Gaussian distribution can describe the radial displacements as ([21], Eq.(7) and Eq.(8)) $\Delta r_x \sim N\left(\frac{\Delta\phi Z}{\cos(\theta)}, 2\sigma_p^2\right)$, $\Delta r_{\tilde{y}} \sim N\left(\frac{\Delta\theta Z}{\cos(\theta)}, 2\sigma_p^2\right)$. Provided that Δr_x and $\Delta r_{\tilde{y}}$ are non-zero mean Gaussian, the pdf of the Rician distribution describes the total radial displacement from the receiver aperture center $\Delta r = \sqrt{\Delta r_x^2 + \Delta r_{\tilde{y}}^2}$ as ([21], Eq.(9))

$$f_{\Delta r|\theta_{xy}}(\Delta r) = \frac{\Delta r}{2\sigma_p^2} \exp\left(-\frac{\Delta r^2 + \theta_{xy}^2}{4\sigma_p^2} \right) I_o\left(\frac{\theta_{xy}\Delta r}{2\sigma_p^2} \right) \tag{13}$$

where $I_o(\cdot)$ represents the modified Bessel function of the first kind with zero order and $\theta_{xy} = \frac{Z}{\cos(\theta)}\sqrt{\Delta\theta^2 + \Delta\phi^2}$. Considering that $\Delta\theta$ and $\Delta\phi$ are zero-mean Gaussian distribution with variance σ_θ^2, the Rayleigh distribution describes the pdf of θ_{xy} as ([21], Eq.(10))

$$f_{\theta_{xy}}(\theta_{xy}) = \frac{\theta_{xy}}{\sigma_{\theta T}^2} \exp\left(-\frac{\theta_{xy}^2}{2\sigma_{\theta T}^2} \right) \tag{14}$$

where $\sigma_{\theta T}^2 = \frac{1}{\theta_{\max}} \int_0^{\theta_{\max}} \frac{\sigma_\theta^2 Z^2}{\cos^2(\theta)} d\theta = \frac{\sigma_\theta^2 Z^2 \tan(\theta_{\max})}{\theta_{\max}}$ represents the average variance over the covered distance. The loss due to pointing error, h_p, can be calculated as ([21], Eq.(11)).

$$h_p \approx A_o \exp\left(\frac{-2\Delta r^2}{w_{d_{eq}}^2} \right) \tag{15}$$

where $A_o = (erf(v))^2$, $v^2 = \frac{\pi a^2}{2w_d^2}$, a represents the receiver radius, $w_d = d\theta_{div}$ indicates the radius of the beam at the receiver plane, and $w_{d_{eq}}^2 = \frac{\sqrt{\pi} w_d^2 erf(v)}{2v\exp(-v^2)}$.

The combined effect of turbulence and pointing errors are defined using the composite fading coefficient $h_2 = h_t h_p h_l$. The PDF of the composite fading model using GG distributed channel is ([21], Eq.(15))

$$f_{h_2}(h) \approx \sum_{i=1}^{n} \frac{C_i h_2^{\frac{\alpha_2+\beta_2}{2}-1}}{2} \mathrm{G}_{0,2}^{2,0}\left(C_P h_2 \Big|_{\frac{\alpha_2-\beta_2}{2}, \frac{\beta_2-\alpha_2}{2}}^{-} \right), \tag{16}$$

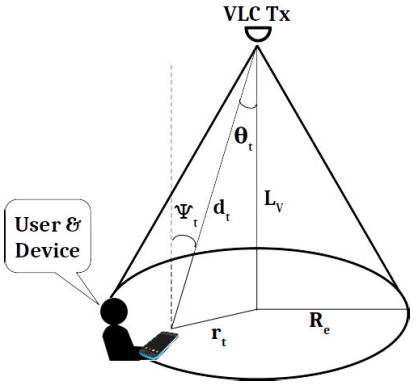

FIGURE 6. VLC channel geometrical representation.

where $C_P = \frac{\alpha_2\beta_2}{A_0} \exp\left(8\frac{x_i^2}{\delta_p^2}\right)$, and

$$C_i = \frac{2\left(\frac{\alpha_2\beta_2}{A_0}\right)^{\frac{\alpha_2+\beta_2}{2}} w_i\delta_\theta^2}{\Gamma(\alpha_2)\Gamma(\beta_2)\delta\delta_p} \times M_{-0.5,0}\left(\frac{x_i^2\delta_p^2}{2\delta^2}\right)\exp\left(x_i^2\left(\frac{4(\alpha_2+\beta_2)}{\delta_p^2}+\frac{\delta_p^2}{4\delta^2}\right)\right),$$

where $\delta_p = \frac{w_{deq}}{\sigma_p}$, $\delta_\theta = \frac{w_{deq}}{\sigma_{\theta T}}$, $\delta^2 = \delta_p^2/2 + \delta_\theta^2/2$ and $M_{(\cdot,\cdot)}(\cdot)$ is the Whittaker M function. x_i and w_i are the Hermite Polynomial ith root and weight of degree n. σ_θ is the UAV-aperture orientation fluctuation standard-deviation and σ_p is the position vibration standard deviation of the UAV and HST.

Using the random variable transformation and after integrating, the SNR CDF of the Eq. (16) is given as

$$F_{\gamma_2}(\gamma) = \frac{1}{\bar{\gamma}_2}\sum_{i=1}^{n}\frac{C_i}{2}\left(\frac{\gamma}{\bar{\gamma}_2}\right)^{\frac{\alpha_2+\beta_2}{4}} \times \mathrm{G}_{1,3}^{2,1}\left(C_P\sqrt{\frac{\gamma}{\bar{\gamma}_2}}\middle|_{\frac{\alpha_2-\beta_2}{2},\frac{\beta_2-\alpha_2}{2},-\frac{\alpha_2+\beta_2}{2}}^{1-\frac{\alpha_2+\beta_2}{2}}\right). \quad (17)$$

The parameter $\bar{\gamma}_2$ in Eq. (17) represents the average SNR of the FSO link between the UAV and train.

C. INSIDE TRAIN

The geometrical representation of VLC channel is depicted in Fig. 6. L_V is the height at which the LED or the VLC Transmitter is placed from the user device. Ψ_t is the angle of incidence and θ_t represents the angle of irradiance. ϕ_C indicates the photodiode field of view (FOV). The euclidian distance d_t of the user device is given by $d_t = (r_t^2 + L_V^2)^{1/2}$ and $cos(\theta_t) = cos(\Psi_t) = L_V/d_t$.

The PDF obtained using the change of variable method for channel gain is given by [48]

$$f_{h_3}(h) = \frac{2}{R_e^2(m_l+3)}(\omega(m_l+1)L_V^{m_l+1})^{\frac{2}{m_l+3}} h_3^{-\frac{2}{m_l+3}-1}, \quad (18)$$

TABLE 3. Binary modulation schemes for ABER parameters.

p	q	Modulation scheme
0.5	0.5	Coherent Binary Frequency Shift Keying (CBFSK)
0.5	1	Coherent Binary Phase Shift Keying (CBPSK)
1	0.5	Non-Coherent Binary Frequency Shift Keying (NBFSK)
1	1	Differential Binary Phase Shift Keying (DBPSK)

where R_e is the maximum radius of the LED's footprint, $m_l = \frac{-ln2}{ln(cos(\theta_{1/2}))}$ is the Lambertian emission order, $\omega = \frac{A}{2\pi}R_p g(\Psi_t)U(\Psi_t)$, A and R_p are the area and responsivity of the photo detector, $U(\Psi_t)$ is gain of the optical filter, and $g(\Psi_t)$ is gain of the optical concentrator and is given as

$$g_{(\Psi_t)} = \begin{cases} \dfrac{n_0^2}{\sin^2\phi_c} & \text{if } 0 \le \Psi_t \le \phi_C, \\ 0 & \text{if } \Psi_t > \phi_c. \end{cases}$$

and, n_0 indicates the refractive index, ϕ_c is the FOV. The PDF of Eq. (18) in terms of instantaneous SNR is given as

$$f_{\gamma_3}(\gamma) = \frac{\bar{\gamma}_3^{\frac{1}{m_l+3}}}{R_e^2(m_l+3)}(\omega(m_l+1)L_V^{m_l+1})^{\frac{2}{m_l+3}}\gamma^{-\frac{m_l+4}{m_l+3}}, \quad (19)$$

where $\gamma_3 = \bar{\gamma}_3 h_t^2$, $\bar{\gamma}_3 = \frac{\rho_1 P_T^2}{N_0 B}$ is the average SNR of the VLC link, P_T is the optical transmit power, N_0 is noise spectral density, and B is the modulation bandwidth. After applying the Binomial approximation and making the mathematical rearrangements, SNR CDF of Eq. (19) is given as [48]

$$F_{\gamma_3}(\gamma) = v_t^N - Nv_t^{N-1}\chi\left(\frac{\gamma}{\bar{\gamma}_3}\right)^{-\frac{1}{m_l+3}}, \quad (20)$$

where N indicates number of access points for VLC, $v_t = 1 + \left(\frac{L_V}{R_e}\right)^2$, and $\chi = \frac{1}{R_e^2}(\omega(m_l+1)L_V^{m_l+1})^{\frac{2}{m_l+3}}$

The end-to-end system CDF of the DF based Triple hop UAV FSO-FSO-VLC cooperative system can be obtained using the equation [48]

$$F_{\gamma_{e2e}}(\gamma) = P_r[\gamma_{e2e} < \gamma] = 1 - \left((1-F_{\gamma_1}(\gamma))(1-F_{\gamma_2}(\gamma))(1-F_{\gamma_3}(\gamma))\right), \quad (21)$$

After substituting the Eqs.(7), (17), and (20) in (21), CDF of the end-to-end system can be written as

$$F_{\gamma_{e2e}}(\gamma) = 1 - \left(1 - \frac{\xi^2 A}{8\pi}\sum_{m=1}^{\beta_1} b_m\, 2^{\alpha_1+m-1}\,\mathrm{G}_{3,7}^{6,1}\left[\frac{B^2}{16}\frac{\gamma}{\mu}\middle|\begin{matrix}X\\Y\end{matrix}\right]\right) \times \left(1 - \frac{1}{\bar{\gamma}_2}\sum_{i=1}^{n}\frac{C_i}{2}\left(\frac{\gamma}{\bar{\gamma}_2}\right)^{\frac{\alpha_2+\beta_2}{4}} \times \mathrm{G}_{1,3}^{2,1}\left(C_P\sqrt{\frac{\gamma}{\bar{\gamma}_2}}\middle|_{\frac{\alpha_2-\beta_2}{2},\frac{\beta_2-\alpha_2}{2},-\frac{\alpha_2+\beta_2}{2}}^{1-\frac{\alpha_2+\beta_2}{2}}\right)\right) \times \left(1 - \left(v_t^N - Nv_t^{N-1}\chi\left(\frac{\gamma}{\bar{\gamma}_3}\right)^{-\frac{1}{m_l+3}}\right)\right). \quad (22)$$

IV. PERFORMANCE EVALUATION

The end-to-end system performance can be evaluated in terms of outage probability and ABER.

A. OUTAGE PROBABILITY ANALYSIS

The probability of end-to-end system output signal to noise ratio (SNR) falls lower than a specified threshold is known as outage probability (OP) can be expressed as [49]

$$P_{out} = P(SNR(h) \leq SNR_{TH}), \tag{23}$$

where SNR_{TH} is the threshold SNR that decides the quality of service (QoS), a threshold is the smallest SNR value above which the QoS is acceptable. The outage probability of the end-to-end system based on DF relay is estimated as

$$\begin{aligned} P_{out} &= F_{\gamma_{e2e}}(\gamma_{th}) \\ &= 1 - \left(1 - \frac{\xi^2 A}{8\pi} \sum_{m=1}^{\beta_1} b_m \, 2^{\alpha_1+m-1} \, \mathrm{G}_{3,7}^{6,1}\left[\frac{B^2}{16}\,\frac{\gamma_{th}}{\mu}\middle|\begin{matrix} X \\ Y \end{matrix}\right]\right) \\ &\quad \times \left(1 - \frac{1}{\bar{\gamma}_2}\sum_{i=1}^{n}\frac{C_i}{2}\left(\frac{\gamma_{th}}{\bar{\gamma}_2}\right)^{\frac{\alpha_2+\beta_2}{4}} \right. \\ &\quad \left. \mathrm{G}_{1,3}^{2,1}\left(C_P\sqrt{\frac{\gamma_{th}}{\bar{\gamma}_2}}\middle|\begin{matrix} 1-\frac{\alpha_2+\beta_2}{2} \\ \frac{\alpha_2-\beta_2}{2}, \frac{\beta_2-\alpha_2}{2}, -\frac{\alpha_2+\beta_2}{2} \end{matrix}\right)\right) \\ &\quad \times \left(1 - \left(v_t^N - N v_t^{N-1}\chi\left(\frac{\gamma_{th}}{\bar{\gamma}_3}\right)^{-\frac{1}{m_l+3}}\right)\right). \end{aligned} \tag{24}$$

B. ABER ANALYSIS

The ABER for different modulation schemes can be calculated using the CDF and is given as ([48],Eq.(18))

$$P_e = \frac{q^p}{2\Gamma(p)}\int_0^\infty \gamma^{p-1}\exp(-q\gamma)F_\gamma(\gamma)d\gamma, \tag{25}$$

C. ABER OF M-DISTRIBUTED LINK

The ABER of the M-distributed link is calculated by substituting Eq. (7) in Eq. (25) and is as follows.

$$\begin{aligned} P_{e1} &= \frac{q^p}{2\Gamma(p)}\int_0^\infty \gamma^{p-1}\exp(-q\gamma) \\ &\quad \cdot \frac{\xi^2 A}{8\pi}\sum_{m=1}^{\beta_1} b_m \, 2^{\alpha_1+m-1} \, \mathrm{G}_{3,7}^{6,1}\left[\frac{B^2}{16}\,\frac{\gamma}{\mu}\middle|\begin{matrix} X \\ Y \end{matrix}\right] d\gamma, \end{aligned} \tag{26}$$

After simplifying the Eq. (26) using the Eqs. (21) and (22) of [50] the ABER of first-hop P_{e1} is given as

$$\begin{aligned} P_{e1} &= \frac{\xi^2 A}{16\pi\Gamma(p)} \\ &\quad \times \sum_{m=1}^{\beta_1} b_m \, 2^{\alpha_1+m-1} \, \mathrm{G}_{4,7}^{6,2}\left[\frac{B^2}{16q\mu}\middle|\begin{matrix} X, 1-p \\ Y \end{matrix}\right]. \end{aligned} \tag{27}$$

TABLE 4. Turbulence parameters used for m-turbulent channel.

Turbulence Region	α_1	β_1	σ_R^2
Weak	11.6	10.1	0.2
Moderate	4.0	1.9	1.6
Strong	4.2	1.4	3.5

D. ABER OF GG-DISTRIBUTED LINK

The ABER of the GG-distributed link is evaluated by substituting Eq. (17) in Eq. (25) which is given as

$$\begin{aligned} P_{e2} &= \frac{q^p}{2\Gamma(p)}\int_0^\infty \gamma^{p-1}\exp(-q\gamma)\cdot\frac{1}{\bar{\gamma}_2}\sum_{i=1}^{n}\frac{C_i}{2}\left(\frac{\gamma}{\bar{\gamma}_2}\right)^{\frac{\alpha_2+\beta_2}{4}} \\ &\quad \times \mathrm{G}_{1,3}^{2,1}\left(C_P\sqrt{\frac{\gamma}{\bar{\gamma}}}\middle|\begin{matrix} 1-\frac{\alpha_2+\beta_2}{2} \\ \frac{\alpha_2-\beta_2}{2}, \frac{\beta_2-\alpha_2}{2}, -\frac{\alpha_2+\beta_2}{2} \end{matrix}\right) d\gamma, \end{aligned} \tag{28}$$

Using the Eqs. (21) and (22) of [50] and making some mathematical manipulations, the Eq. (28) can be re-written as

$$P_{e2} = \frac{q^{-\frac{\alpha_2+\beta_2}{4}}}{16\pi\Gamma(p)\bar{\gamma}_2}\sum_{i=1}^{n}\frac{C_i}{\bar{\gamma}_2^{\frac{\alpha_2+\beta_2}{4}}}\mathrm{G}_{3,6}^{4,3}\left(\frac{C_P^2}{16q}\middle|\begin{matrix} X1 \\ Y1 \end{matrix}\right), \tag{29}$$

Here

$$\begin{aligned} X1 &= \frac{1}{2} - \frac{\alpha_2+\beta_2}{4}, 1 - \frac{\alpha_2+\beta_2}{4}, 1-p-\frac{\alpha_2+\beta_2}{4}, \text{ and} \\ Y1 &= \frac{\alpha_2-\beta_2}{4}, \frac{\alpha_2-\beta_2}{4}+\frac{1}{2}, \frac{\beta_2-\alpha_2}{4}, \frac{\beta_2-\alpha_2}{4}+\frac{1}{2}, \\ &\quad -\frac{\alpha_2+\beta_2}{4}, -\frac{\alpha_2+\beta_2}{4}+\frac{1}{2}. \end{aligned}$$

E. ABER OF VLC LINK

The ABER of the VLC link is calculated by substituting Eq. (20) in Eq. (25) and is given as

$$\begin{aligned} P_{e3} &= \frac{q^p}{2\Gamma(p)}\int_0^\infty \gamma^{p-1}\exp(-q\gamma) \\ &\quad \cdot\left(v_t^N - N v_t^{N-1}\chi\left(\frac{\gamma}{\bar{\gamma}_3}\right)^{-1/m_l+3}\right)d\gamma, \end{aligned} \tag{30}$$

Using the Eqs. (21) and (22) of [50] the Eq. (30) can be re-written, after making some mathematical manipulations as

$$P_{e3} = \frac{v_t^N}{2} - \frac{N}{2\Gamma(p)}v_t^{N-1}\chi\left(\frac{q}{\bar{\gamma}_3}\right)^{\frac{-1}{m_l+3}}\Gamma\left(p-\frac{1}{m_l+3}\right). \tag{31}$$

The ABER of the DF triple-hop UAV-based FSO-FSO-VLC cooperative system can be given as

$$P_{e2e} = 1 - ((1-P_{e1})(1-P_{e2})(1-P_{e3})), \tag{32}$$

After substituting Eqs.(27), (29), and (31) in Eq.(32) the end-to-end ABER can be given as

$$\begin{aligned} &P_{e2e} \\ &= 1 - \left(1 - \frac{\xi^2 A}{16\pi\Gamma(p)}\sum_{m=1}^{\beta_1} b_m \, 2^{\alpha_1+m-1} \, \mathrm{G}_{4,7}^{6,2}\left[\frac{B^2}{16q\mu}\middle|\begin{matrix} X, 1-p \\ Y \end{matrix}\right]\right) \end{aligned}$$

TABLE 5. Parameters used for triple-hop UAV-based FSO-FSO-VLC cooperative system.

FSO Parameter	Value
Link length, L	1 Km
FSO Wavelength, λ	1550 nm
UAV altitude, Z	1.5 Km
Coverage distance of train track, L_c	6 Km
Beam divergence, θ_{div}	1 mrad
VLC Parameter	**Value**
Photodiode responsivity, R_p	0.5
Height of the LED Transmitter, L_V	1.5 m
Transmission semi angle at half power, $\theta_{1/2}$	30^0
Photodiode FOV, ϕ_c	45^0
Photodetector area, A	5 cm^2
Gain of optical filter, $U(\Psi_t)$	0.9
Refractive index, n_0	1
No of access points, N	2
Maximum radius of the LED cell footprint, R_e	5 m
Data Rate	1 Gbps

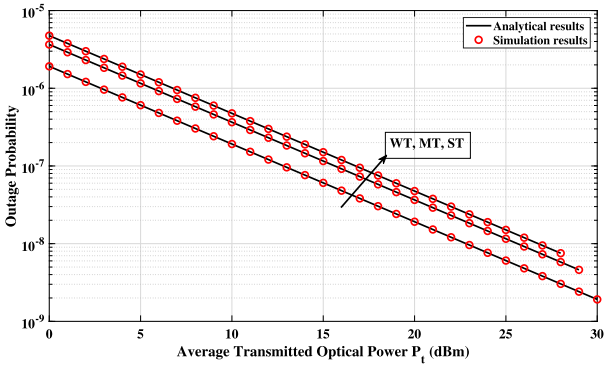

FIGURE 7. Outage probability vs average transmitted optical power for different FSO turbulence conditions.

$$\times\left(1-\frac{q^{-\frac{\alpha_2+\beta_2}{4}}}{16\pi\Gamma(p)\bar{\gamma}_2}\sum_{i=1}^{n}\frac{C_i}{\bar{\gamma}_2^{\frac{\alpha_2+\beta_2}{4}}}\,\mathrm{G}_{3,6}^{4,3}\left(\frac{C_P^2}{16q}\middle|_{Y1}^{X1}\right)\right)$$
$$\times\left(1-\left(\frac{v_t^N}{2}-\frac{N}{2\Gamma(p)}v_t^{N-1}\chi\left(\frac{q}{\bar{\gamma}_3}\right)^{\frac{-1}{m_l+3}}\Gamma\left(p-\frac{1}{m_l+3}\right)\right)\right). \quad (33)$$

V. RESULTS AND DISCUSSIONS

In this section, the numerical results for the outage probability and the average BER for a triple-hop UAV based FSO-FSO-VLC cooperative system are analyzed and validated using Monte-Carlo simulations.The FSO link from the gateway to the UAV is modeled as M-turbulent channel with a link length $L = 1$ km and wavelength $\lambda = 1550$ nm. The turbulence parameters used are mentioned in Table 4 from [51]. The UAV to the HST is modeled as a FSO channel using Gamma Gamma distribution with altitudes Z=(1.5,2,2.5) km and coverage distances of L_c=(6,10) km of train track with beam divergence θ_{div} = (1,1.5) mrad. The turbulence parameters are accordingly calculated as (α_2=6.3 and β_2=6). The vibrations of the UAV and HST are considered as $\sigma_p = (250,350)$ mm. The UAV aperture orientation fluctuations standard-deviation is σ_θ=(0.5,1) mrad. The HST to the user's device is modeled as a VLC link with transmitter half power semi-angle $\theta_{1/2} = 30^0$ and number of access points as 2. The distance between the LED and the user is L_V=1.5 m. The average SNR of all the links are assumed to be $\gamma_{th} = 10$ dB.

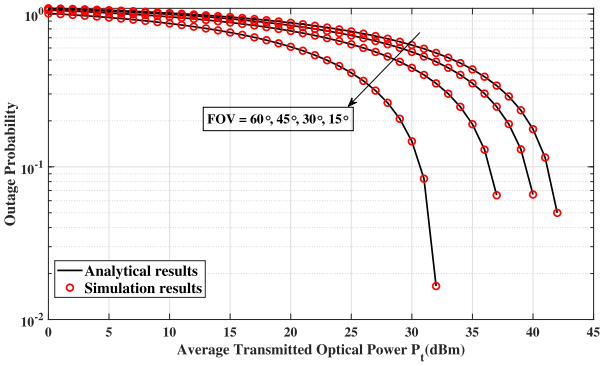

FIGURE 8. Outage probability vs average transmitted optical power for the triple hop UAV based FSO-FSO-VLC cooperative system for different FOV Values.

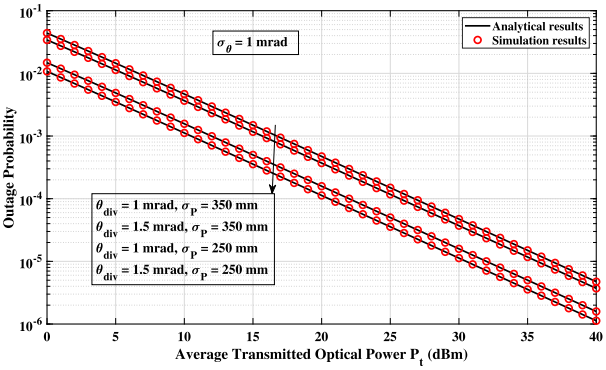

FIGURE 9. Outage probability vs average transmitted optical power for the UAV based FSO communications with θ_{div} = (1, 1.5) mrad, σ_p = (250, 350) mm, σ_θ = 1 mrad.

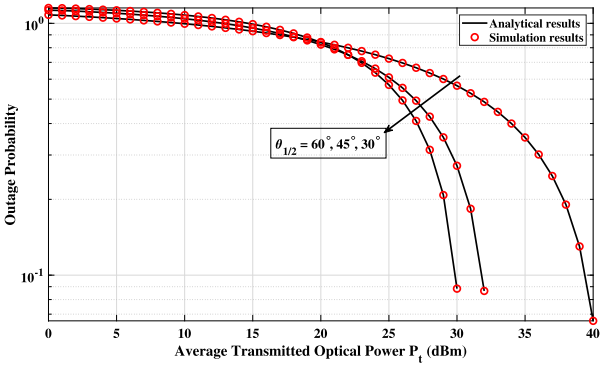

FIGURE 10. Outage probability vs average transmitted optical power for the triple hop UAV based FSO-FSO-VLC cooperative system for different transmitter half power semi-angle.

The outage probability versus average transmitted optical power (in dBm)for different FSO turbulence conditions is shown in Fig. 7.As seen from the figure outage probability is higher in strong turbulence conditions as compared to moderate and weak turbulences.At P_t=20 dBm, the outage probability is 2.692×10^{-8} and 5.425×10^{-8} for moderate and strong turbulences respectively.

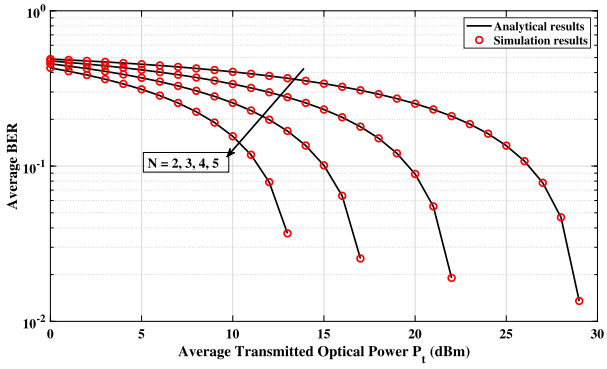

FIGURE 11. Average BER vs average transmitted optical power for the triple hop UAV based FSO-FSO-VLC cooperative system by varying the number of access points.

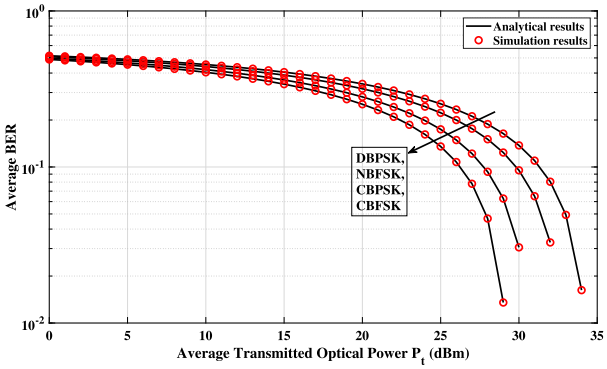

FIGURE 12. Average BER vs average transmitted optical power for the triple hop UAV based FSO-FSO-VLC cooperative system for different modulation techniques.

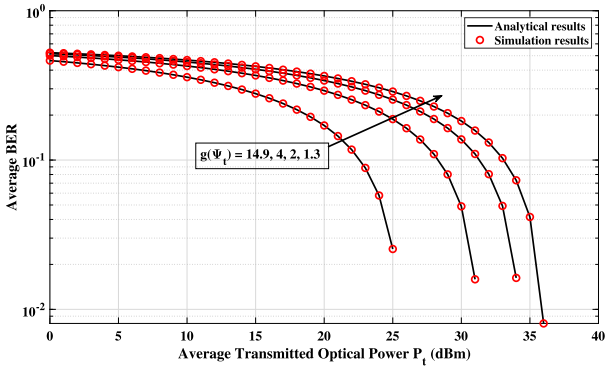

FIGURE 13. Average BER vs average transmitted optical power for the triple hop UAV based FSO-FSO-VLC cooperative system with different gain of optical concentrator.

The outage probability versus average transmitted optical power (in dBm)for a triple-hop UAV based FSO-FSO-VLC cooperative system with different FOV of the photodetector for weak turbulence condition is presented in Fig. 8. It can be observed from the plot that, when we increase the FOV, the outage probability increases.The photodetector concentrator power increases, with decrease in FOV, thereby decreasing the outage probability of the triple hop UAV based FSO-FSO-VLC cooperative system.A receiver with narrow FOV outperforms receiver with wide FOV since it is more susceptible to ambient light noise.At P_t=30 dBm, the outage probability for the considered system at L=1.5 m, and FOV = 15^0, FOV = 30^0 are 1.467×10^{-1} and 4.445×10^{-1} respectively.

Fig. 9 shows the outage probability versus average transmitted optical power (in dBm) for a UAV based FSO system with altitude Z=1.5 km and coverage distance L_c=6 km of train track. The position vibration standard deviation of the UAV is varied between σ_p= (250,350) mm and the beam divergence values between θ_{div} = (1,1.5) mrad. The UAV orientation fluctuation standard deviation is taken as σ_θ=1 mrad. It is revealed that when σ_p fluctuates from 250 mm to 350 mm, the outage probability increases for a particular transmitted optial power of 10 dBm. It is also inferred that when the beam divergence is increased from θ_{div} = 1 mrad to 1.5 mrad, the outage probability sligthly decreases. High degradation in the outage performance is observed owing to the fluctuations in the UAV position and orientation and also HST position variations. Increase in the beam divergence aids in the reduction of fluctuations due to UAV aperture orientation.

In Fig. 10, the outage probability versus average transmitted optical power (in dBm) for a triple-hop UAV based FSO-FSO-VLC cooperative system with different transmitter half power semi-angle is presented. The outage probability of the considered system decreases with increase in the transmitter half power semi-angle. At P_t = 30 dBm, the outage probability for the considered system at $\theta_{1/2}$ = 30^0 and $\theta_{1/2}$ = 60^0 are 5.65×10^{-1} and 8.84×10^{-2} respectively.

To extend our study for the triple hop UAV based FSO-FSO-VLC cooperative system, we present in Fig. 11, average BER versus average transmitted optical power (in dBm) by varying the LED luminaries. It can be clearly observed that the average BER decreases with increase in the number of LED's installed on the ceiling. For example, at P_t=10 dBm, the average BER for the considered system at N=3 and N=5 are 3.375×10^{-1} and 1.555×10^{-1} respectively.

In Fig. 12, we examine the Average BER versus average transmitted optical power (in dBm) for different modulation schemes considering L = 1.5 m and FOV=45^0. The trend of curves clearly indicates that CBFSK outperforms other modulation techniques.

Fig. 13 presents the Average BER versus average transmitted optical power (in dBm) for different gain of the optical concentrator. We observe that the average BER decreases with increase in the gain of the optical concentrator.

VI. CONCLUSION

This paper proposes a novel triple-hop UAV-based FSO-FSO-VLC cooperative system for high-speed internet connectivity in high-speed trains. Analytical expressions for the statistical characteristics of Average transmitted optical power of the triple-hop system are derived. These statistical characteristics are applied in deriving new analytical expressions for Outage probability and ABER of the proposed triple-hop UAV-based

FSO-FSO-VLC system. Results revealed that the system with lesser FOV and increased half power semi-angle offers better outage performance at low transmitted optical power. The ABER of the proposed system improves when the number of access points used are less with minimum gain of the optical concentrator at high optical transmit power. It is also noticed that the proposed system outperforms with CBFSK while comparing other modulation schemes. The challenges due to UAV aperture and HST alignment can be improved by adjusting the beam divergence angle. Thus the proposed system looks greatly feasible and provides a desirable solution to the high-speed internet connectivity issues in high-speed trains. In the future, this work may be extended to analyse the secrecy performance of the FSO communication and VLC systems while considering different eavesdropping scenarios dependent on the location of the eavesdropper.

REFERENCES

[1] D. T. Fokum and V. S. Frost, "A survey on methods for broadband Internet access on trains," *IEEE Commun. Surveys Tuts.*, vol. 12, no. 2, pp. 171–185, 2nd Quart., 2010.

[2] M. Aguado, O. Onandi, P. S. Agustin, M. Higuero, and E. J. Taquet, "WiMax on rails," *IEEE Veh. Technol. Mag.*, vol. 3, no. 3, pp. 47–56, Sep. 2008.

[3] A. K. Majumdar, *Advanced Free Space Optics (FSO): A Systems Approach*, vol. 186. Cham, Switzerland: Springer, 2014.

[4] Z. Ghassemlooy, W. Popoola, and S. Rajbhandari, *Optical Wireless Communications: System and Channel Modelling With MATLAB*. Boca Raton, FL, USA: CRC Press, 2019.

[5] W. Liu, J. Ding, J. Zheng, X. Chen, and C.-L. I, "Relay-assisted technology in optical wireless communications: A survey," *IEEE Access*, vol. 8, pp. 194384–194409, 2020.

[6] K. Mori, M. Terada, K. Nakamura, R. Murakami, K. Kaneko, F. Teraoka, D. Yamaguchi, and S. Haruyama, "Fast handover mechanism for high data rate ground-to-train free-space optical communication system," in *Proc. IEEE Globecom Workshops (GC Wkshps)*, Dec. 2014, pp. 499–504.

[7] R. Paudel, Z. Ghassemlooy, H. Le-Minh, and S. Rajbhandari, "Modelling of free space optical link for ground-to-train communications using a Gaussian source," *IET Optoelectron.*, vol. 7, no. 1, pp. 1–8, Feb. 2013.

[8] Y. Kaymak, R. Rojas-Cessa, J. Feng, N. Ansari, and M. Zhou, "On divergence-angle efficiency of a laser beam in free-space optical communications for high-speed trains," *IEEE Trans. Veh. Technol.*, vol. 66, no. 9, pp. 7677–7687, Sep. 2017.

[9] Y. Kaymak, R. Rojas-Cessa, J. Feng, N. Ansari, M. Zhou, and T. Zhang, "A survey on acquisition, tracking, and pointing mechanisms for mobile free-space optical communications," *IEEE Commun. Surveys Tuts.*, vol. 20, no. 2, pp. 1104–1123, 2nd Quart., 2018.

[10] D. Sanz, "Satellite technologies for broadband Internet access onboard high speed trains," in *Proc. 7th World. Congr. Railway Res.* 2006, pp. 1–9.

[11] F. Zou, X. Jiang, and Z. Lin, "IEEE 802.20 based broadband railroad digital network–the infrastructure for M-commerce on the train," *Generations*, vol. 3, pp. 771–776, 2004.

[12] B. Lannoo, D. Colle, M. Pickavet, and P. Demeester, "Radio-over-fiber-based solution to provide broadband Internet access to train passengers [topics in optical communications]," *IEEE Commun. Mag.*, vol. 45, no. 2, pp. 56–62, Feb. 2007.

[13] K. Ishizu, M. Kuroda, and H. Harada, "Bullet-train network architecture for broadband and real-time access," in *Proc. IEEE Symp. Comput. Commun.*, Jul. 2007, pp. 241–248.

[14] S. Haruyama, H. Urabe, T. Shogenji, S. Ishikawa, M. Hiruta, F. Teraoka, T. Arita, H. Matsubara, and S. Nakagawa, "New ground-to-train high-speed free-space optical communication system with fast handover mechanism," in *Proc. Opt. Fiber Commun. Conf. Expo. Nat. Fiber Optic Eng. Conf.*, Mar. 2011, pp. 1–3.

[15] W. Zeng, J. Zhang, K. P. Peppas, B. Ar, and Z. Zhong, "UAV-aided wireless information and power transmission for high-speed train communications," in *Proc. 21st Int. Conf. Intell. Transp. Syst. (ITSC)*, Nov. 2018, pp. 3409–3414.

[16] Y. Min Park, Y. Kyaw Tun, Z. Han, and C. Seon Hong, "Trajectory optimization and phase-shift design in IRS assisted UAV network for high speed trains," 2021, *arXiv:2107.00857*.

[17] Y. Zhou, "Future communication model for high-speed railway based on unmanned aerial vehicles," 2014, *arXiv:1411.3450*.

[18] Y. M. Park, Y. K. Tun, and C. S. Hong, "Optimized deployment of multi-UAV based on machine learning in UAV-HST networking," in *Proc. 21st Asia–Pacific Netw. Oper. Manage. Symp. (APNOMS)*, Sep. 2020, pp. 102–107.

[19] N. Mohan, Z. Ghassemlooy, S. Zvanovec, M. M. Abadi, R. Hudson, and M. R. Bhatnagar, "Relayed FSO links for ground-to-train communications," in *Proc. 12th Int. Symp. Commun. Syst., Netw. Digit. Signal Process. (CSNDSP)*, Jul. 2020, pp. 1–6.

[20] Q. Fan, N. Ansari, J. Feng, R. Rojas-Cessa, M. Zhou, and T. Zhang, "Reducing the number of FSO base stations with dual transceivers for next-generation ground-to-train communications," *IEEE Trans. Veh. Technol.*, vol. 67, no. 11, pp. 11143–11153, Nov. 2018.

[21] H. S. Khallaf and M. Uysal, "UAV-based FSO communications for high speed train backhauling," in *Proc. IEEE Wireless Commun. Netw. Conf. (WCNC)*, Apr. 2019, pp. 1–6.

[22] H. S. Khallaf and M. Uysal, "Comprehensive study on UAV-based FSO links for high-speed train backhauling," *Appl. Opt.*, vol. 60, no. 27, pp. 8239–8247, 2021.

[23] V. R. Nallagonda and P. Krishnan, "Bit error rate analysis of polarization shift keying based free space optical link over different weather conditions for inter unmanned aerial vehicles communications," *Opt. Quantum Electron.*, vol. 53, no. 9, pp. 1–15, Sep. 2021.

[24] V. R. Nallagonda and P. Krishnan, "Performance analysis of FSO based inter-UAV communication systems," *Opt. Quantum Electron.*, vol. 53, no. 4, pp. 1–20, Apr. 2021.

[25] I. Swamidoss, A. Almarzooqi, A. A. AlMansoori, and S. Sayadi, "Average spectral efficiency analysis of FSO communication link over atmospheric turbulence channel using various modulation techniques for UAV application," *Proc. SPIE*, vol. 11153, Oct. 2019, Art. no. 111530N.

[26] A. Almarzooqi, I. Swamidoss, A. A. AlMansoori, and S. Sayadi, "BER analysis of FSO communication link over UAE weather conditions for UAV applications," *Proc. SPIE*, vol. 11153, Oct. 2019, Art. no. 111530J.

[27] M. T. Dabiri, S. M. S. Sadough, and M. A. Khalighi, "Channel modeling and parameter optimization for hovering UAV-based free-space optical links," *IEEE J. Sel. Areas Commun.*, vol. 36, no. 9, pp. 2104–2113, Sep. 2018.

[28] M. Najafi, H. Ajam, V. Jamali, P. D. Diamantoulakis, G. K. Karagiannidis, and R. Schober, "Statistical modeling of the FSO fronthaul channel for UAV-based communications," *IEEE Trans. Commun.*, vol. 68, no. 6, pp. 3720–3736, Jun. 2020.

[29] J.-Y. Wang, Y. Ma, R.-R. Lu, J.-B. Wang, M. Lin, and J. Cheng, "Hovering UAV-based FSO communications: Channel modelling, performance analysis, and parameter optimization," *IEEE J. Sel. Areas Commun.*, vol. 39, no. 10, pp. 2946–2959, Oct. 2021.

[30] M. Taheri, N. Ansari, J. Feng, R. Rojas-Cessa, and M. Zhou, "Provisioning internet access using FSO in high-speed rail networks," *IEEE Netw.*, vol. 31, no. 4, pp. 96–101, Jul. 2017.

[31] G. Xu, N. Zhang, M. Xu, Z. Xu, Q. Zhang, and Z. Song, "Outage probability and average BER of UAV-assisted dual-hop FSO communication with amplify-and-forward relaying," *IEEE Trans. Veh. Technol.*, pp. 1–16, 2023.

[32] M. Xu, G. Xu, Y. Dong, W. Wang, Q. Zhang, and Z. Song, "UAV-assisted FSO communication system with amplify-and-forward protocol under AOA fluctuations: A performance analysis," *China Commun.*, early access, May 10, 2023, doi: 10.23919/JCC.ea.2022-0528.202302.

[33] E. T. Michailidis, P. S. Bithas, N. Nomikos, D. Vouyioukas, and A. G. Kanatas, "Outage probability analysis in multi-user FSO/RF and UAV-enabled MIMO communication networks," *Phys. Commun.*, vol. 49, Dec. 2021, Art. no. 101475.

[34] R.-R. Lu, J.-Y. Wang, X.-T. Fu, S.-H. Lin, Q. Wang, and B. Zhang, "Performance analysis and optimization for UAV-based FSO communication systems," *Phys. Commun.*, vol. 51, Apr. 2022, Art. no. 101594.

[35] Y. Wu, D. Kong, Q. Wang, and G. Li, "Performance analysis of UAV-assisted hybrid FSO/RF communication systems under various weather conditions," *Sensors*, vol. 23, no. 17, p. 7638, Sep. 2023.
[36] R. Paudel, Z. Ghassemlooy, H. Le-Minh, S. Rajbhandari, and B. Livingstone, "Investigation of FSO ground-to-train communications in a laboratory environment," in *Proc. 2nd Asian Himalayas Int. Conf. Internet (AH-ICI)*, Nov. 2011, pp. 1–5.
[37] Q. Fan, M. Taheri, N. Ansari, J. Feng, R. Rojas-Cessa, M. Zhou, and T. Zhang, "Reducing the impact of handovers in Ground-to-Train free space optical communications," *IEEE Trans. Veh. Technol.*, vol. 67, no. 2, pp. 1292–1301, Feb. 2018.
[38] S. Fathi-Kazerooni, Y. Kaymak, R. Rojas-Cessa, J. Feng, N. Ansari, M. Zhou, and T. Zhang, "Optimal positioning of ground base stations in free-space optical communications for high-speed trains," *IEEE Trans. Intell. Transp. Syst.*, vol. 19, no. 6, pp. 1940–1949, Jun. 2018.
[39] W. A. Mabrouk, M. F. L. Abdullah, and M. S. M. Gismalla, "Enhancement of link range for FSO ground to train communications using multiple transmitters concept," in *Proc. Int. Conf. Inf. Sci. Commun. Technol. (ICISCT)*, Mar. 2019, pp. 1–7.
[40] A. Gupta, N. Sharma, P. Garg, and M.-S. Alouini, "Cascaded FSO-VLC communication system," *IEEE Wireless Commun. Lett.*, vol. 6, no. 6, pp. 810–813, Dec. 2017.
[41] P. Pesek, S. Zvánovec, P. Chvojka, Z. Ghassemlooy, and P. A. Haigh, "Demonstration of a hybrid FSO/VLC link for the last mile and last meter networks," *IEEE Photon. J.*, vol. 11, no. 1, pp. 1–7, Feb. 2019.
[42] M. Petkovic, A. Cvetkovic, and M. Narandzic, "Outage probability analysis of RF/FSO-VLC communication relaying system," in *Proc. 11th Int. Symp. Commun. Syst., Netw. Digit. Signal Process. (CSNDSP)*, Jul. 2018, pp. 1–5.
[43] L. Bhargava Kumar, P. N. Ramavath, P. Krishnan, and A. K. Majumdar, "Underwater wireless optical communications based reconfigurable UOWSN for monitoring and discovering continental margin ore deposits," *Appl. Opt.*, vol. 61, no. 11, p. 3141, 2022.
[44] A. Jurado-Navas, J. M. Garrido-Balsells, J. F. Paris, A. Puerta-Notario, and J. Awrejcewicz, "A unifying statistical model for atmospheric optical scintillation," in *Numerical Simulations of Physical and Engineering Processes*, vol. 181. Rijeka, Croatia: Intech, 2011.
[45] I. S. Ansari, F. Yilmaz, and M.-S. Alouini, "Performance analysis of free-space optical links over Málaga $\mathcal{M}$ turbulence channels with pointing errors," *IEEE Trans. Wireless Commun.*, vol. 15, no. 1, pp. 91–102, Jan. 2016.
[46] G. Aarthi, K. Prabu, and G. R. Reddy, "Aperture averaging effects on the average spectral efficiency of FSO links over turbulence channel with pointing errors," *Opt. Commun.*, vol. 385, pp. 136–142, Feb. 2017.
[47] M. A. Al-Habash, "Mathematical model for the irradiance probability density function of a laser beam propagating through turbulent media," *Opt. Eng.*, vol. 40, no. 8, p. 1554, Aug. 2001.
[48] R. Deka and S. Anees, "Performance analysis of DF based cascaded VLC-FSO-VLC system," in *Proc. 3rd Int. Conf. Adv. Commun. Technol. Netw. (CommNet)*, Sep. 2020, pp. 1–6.
[49] K. Prabu, D. S. Kumar, and T. Srinivas, "Performance analysis of FSO links under strong atmospheric turbulence conditions using various modulation schemes," *Optik*, vol. 125, no. 19, pp. 5573–5581, Oct. 2014.
[50] V. S. Adamchik and O. I. Marichev, "The algorithm for calculating integrals of hypergeometric type functions and its realization in REDUCE system," in *Proc. Int. Symp. Symbolic Algebr. Comput.*, Jul. 1990, pp. 212–224.
[51] W. M. R. Shakir, "Performance evaluation of a selection combining scheme for the hybrid FSO/RF system," *IEEE Photon. J.*, vol. 10, no. 1, pp. 1–10, Feb. 2018.

AARTHI GUNASEKAR received the bachelor's degree in electronics and communication engineering from Madras University, and the M.Tech. degree in communication engineering and the Ph.D. degree from the Vellore Institute of Technology, Vellore, India. She is currently an Associate Professor with the School of Electronics Engineering, Vellore Institute of Technology. She has four years of industrial experience and 13 years of teaching experience. Her research interests include wireless optical communication (FSO and VLC), optical communication, wireless communication, optical sensors, and 5G.

L. BHARGAVA KUMAR received the master's degree from Jawaharlal Nehru Technological University Anantapur, Andhra Pradesh, India, and the Ph.D. degree from the National Institute of Technology Karnataka, Surathkal, India. He is with the Department of Electronics and Communication Engineering, BVRIT Hyderabad College of Engineering for Women, Hyderabad, India. His research interests include optical and wireless communication, free-space optical communication, and underwater optical wireless communication.

PRABU KRISHNAN (Senior Member, IEEE) received the Ph.D. degree in free space optical communication from the Department of Electronics and Communication Engineering, NIT, Tiruchirappalli, India. Currently, he is an Assistant Professor with the Department of Electronics and Communication Engineering, National Institute of Technology Karnataka, Surathkal, India. He has been recognized as one of the world's top 2% researchers for the years 2019 and 2020. His research interests include optical wireless communications, radio over free space optical communications, radio over fiber, optical sensors, and nano-photonics.

RAJESH NATARAJAN received the bachelor's degree in electronics and communications engineering, the master's degree in communication systems, and the Ph.D. degree from Anna University, Chennai. Currently, he is an Assistant Professor (Senior) with the School of Electronics Engineering, Vellore Institute of Technology, Vellore. He has two years of industrial experience and ten years of teaching experience in reputed private institutions. His research interests include the design and analysis of UWB antennas, frequency selective surfaces and planar transmission lines, and wireless optical communication. He has published 18 journal articles in reputed journals and 15 conference publications.

DUSHANTHA NALIN K. JAYAKODY (Senior Member, IEEE) received the M.Sc. degree in electronics and communications engineering from the Department of Electrical and Electronics Engineering, Eastern Mediterranean University, Turkey (under the University Full Graduate Scholarship), and the Ph.D. degree in electronics and communications engineering from the University College Dublin, Ireland. From 2014 to 2016, he was a Postdoctoral Research Fellow with the University of Tartu, Estonia, and University of Bergen, Norway. Since 2021, he has been with the Autonoma TechLab, Portugal, and Universidade Autonoma de Lisboa, Portugal. He was also the Head of the School of Postgraduate Research, Sri Lanka Technological Campus (SLTC), Padukka Sri Lanka, where he was also the Founding Head of the Centre of Telecommunication Research. Since 2016, he has been a Professor with the School of Computer Science Robotics, National Research Tomsk Polytechnic University (TPU), Russia. He has 200 international peer reviewed journals and conference papers and books. His research interests include PHY and NET layer prospective of 5G communications technologies. In his career, so far, he has attracted nearly 6M USD research funding. He has organized or co-organized more than 30 workshops, special sessions, and IEEE conferences. He also serves as an Area Editor for the *Physical Communications* journal (Elsevier), *Information* journal (MDPI), *Sensors* (MDPI), and *Internet of Technology Letters* (Wiley). Also, he serves on the Advisory Board of *Multidisciplinary Journal Sciences* (MDPI). He is a fellow of IET.